Extreme Mechanics Letters 41 (2020) 101049

Contents lists available at ScienceDirect

Extreme Mechanics Letters

journal homepage: www.elsevier.com/locate/eml

Mechanics tuning of liquid inclusions via bio-coating

Xin Chen [a,b,e,*], Moxiao Li [b,c,e], Shaobao Liu [d,e], Wei He [b], Fei Ti [d,e], Yuqing Dong [c,f], Guy M. Genin [c,f,g], Feng Xu [c,f,**], Tian Jian Lu [d,e,***]

[a] Xi'an Modern Chemistry Research Institute, Xi'an, 710065, PR China
[b] State Key Laboratory for Strength and Vibration of Mechanical Structures, Xi'an Jiaotong University, Xi'an 710049, PR China
[c] Bioinspired Engineering and Biomechanics Center (BEBC), Xi'an Jiaotong University, Xi'an 710049, PR China
[d] State Key Laboratory of Mechanics and Control of Mechanical Structures, Nanjing University of Aeronautics and Astronautics, Nanjing 210016, PR China
[e] Nanjing Center for Multifunctional Lightweight Materials and Structures (MLMS), Nanjing University of Aeronautics and Astronautics, Nanjing 210016, PR China
[f] The Key Laboratory of Biomedical Information Engineering of Ministry of Education, Xi'an Jiaotong University, Xi'an 710049, PR China
[g] National Science Foundation Science and Technology Center for Engineering Mechanobiology, Washington University, St. Louis, MO 63130, USA

ARTICLE INFO

Article history:
Received 23 August 2020
Received in revised form 26 September 2020
Accepted 14 October 2020
Available online 17 October 2020

Keywords:
Inclusion theory
Cell mechanics
Stiffness gradient
Liquid inclusion

ABSTRACT

Liquid-like inclusions arising in biomaterials and tissues often have coatings with material properties that differ from those of both the inclusion and the surrounding matrix. Understanding how these coatings interact with the inclusion and the surrounding matrix is critical to understanding tissue function and to developing a class of biomimetic materials. We therefore developed a closed-form mathematical solution to characterize how the properties of a coating surrounding a spherical liquid-like inclusion affect the volumetric strain it experiences when the surrounding matrix is loaded uniaxially. Results show that the coating can amplify or attenuate the volumetric strain within the liquid inclusion, depending upon the relative properties of the inclusion, coating, and matrix. We used the solution to study amplification and attenuation of mechanical fields in healthy and diseased tissues, and found that pathological remodeling of coatings can have a tremendous impact on the mechanical fields experienced by living cells. Results suggest important roles for coatings surrounding living cells in tuning the mechanobiology cues transmitted to cells when the tissues that host them are loaded mechanically.

1. Introduction

Many functional units in biology can manifest as liquid-like inclusions at certain stages of development and remodeling, including cells within tissues and organelles within cells (Fig. 1). Responses of these inclusions to mechanical loading of the surrounding matrix are critical to biological function [1–5]. For instance, cells within solid tissues often create a pericellular region of matrix around them, which can be approximated mechanically as a coating arising from extracellular matrix (ECM) production and remodeling [6], or from contraction of cells such as fibroblasts [7,8], smooth muscle cells [8,9], or certain cancer cells [10] (Fig. 1). Mechanical properties of the coating and ECM can change in response to disease, connections to neighboring cells, or further remodeling [11–13]. In diseases such as fibrosis and certain cancers, the coatings of cells can change dramatically from the healthy phenotype [14,15]. This led us to ask whether a coating surrounding a cell or group of cells could be tuned by a healthy cell as a component of homeostatic regulation.

Our approach was to use a continuum model and idealized system to best understand the scaling laws associated with stiffening and enlarging the coating. The study of coated inclusions dates back to the work of Walpole [17], which was further developed to analyze the stress concentration around an inclusion [18–20]. The model has also been adapted to predict the homogenized properties of composites containing coated inclusions embedded in an elastic matrix [21–24], and to design a range of functional materials [25–27]. The concept of a coated inclusion underlies the generalized self-consistent method to predict the effective properties of a composite containing a high volume fraction of inclusions [28–31]. However, these models are not suitable for

* Correspondence to: No. 165, Zhangbadong Road, Xi'an, Shanxi, 710065, PR China.
** Correspondence to: No. 28, Xianning West Road, Xi'an, Shaanxi, 710049, PR China.
*** Correspondence to: No. 29, Yudao Street, Nanjing, Jiangsu, 210016, PR China.
E-mail addresses: xinchern@126.com (X. Chen), fengxu@xjtu.edu.cn (F. Xu), tjlu@nuaa.edu.cn (T.J. Lu).

https://doi.org/10.1016/j.eml.2020.101049
2352-4316/

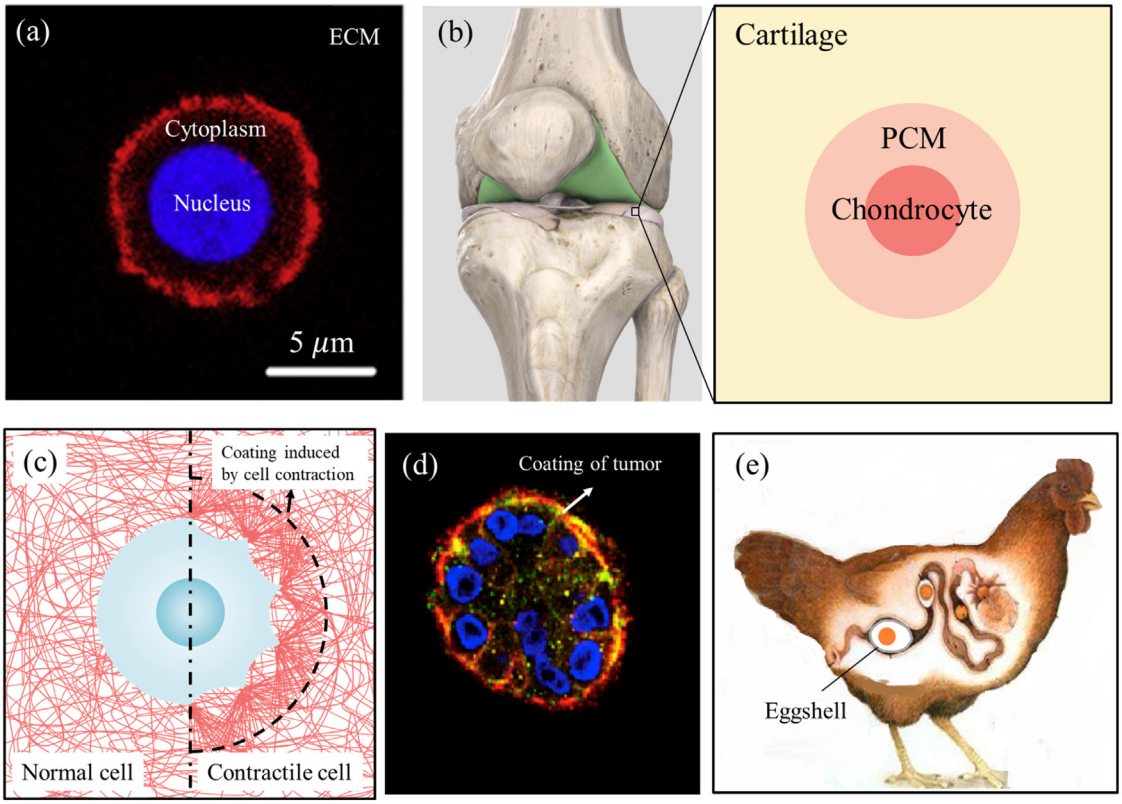

Fig. 1. Examples of a coated inclusion embedded in a three-dimensional matrix. (a) For a cell in a three-dimensional environment [16], the nucleus, cytoplasm and extracellular matrix are regarded as the inclusion, coating and matrix, respectively. Some cells can remodel their microenvironments to create a pericellular matrix coating surrounding them. For instance, (b) chondrocytes [6] and (c) myofibroblasts. (d) Certain tumors are surrounded by dense extracellular matrix proteins [14]. (e) An egg is protected from pressure by a shell; a pericellular coating of proteins can act similarly.

the purposes of the present study because they are not applicable to liquid inclusions, and furthermore have not explored the biomechanics ramifications of the problem.

We therefore developed a mechanical model to investigate the deformation of coated fluid-filled inclusions in elastic bodies. Using the stress potential function method, we derived explicit expressions for the elastic fields and investigated how the stiffness and thickness of the coating influence the volumetric strain experienced by the inclusion. We then applied the solution to assess the ways that a coating could be modified to tune the mechanical fields felt by a cell, and to understand how cells, cell aggregates, and subcellular organelles tailor their coatings in both physiologic and pathophysiologic conditions. Our results suggest that cells can tailor the degree to which the mechanical stimuli that they experience are amplified or attenuated through tuning of the thickness or stiffness of their protein coatings.

2. Problem statement

Although previous treatments of cells or cell aggregates in elastic matrices often treat cells as solids [32–34], cells undergoing stretch typically transit to a fluid-like state [35–38]. Cells also fluidize to various degrees under cyclic loading [39,40], and are in general compressible [41]. We therefore studied spherical liquid inclusions coated with a solid coating embedded in an infinite elastic matrix (Fig. 2). We show in Section 6 that the effect of the coating is the same for both liquid and solid inclusions, and then apply the solution to study a range of tissues.

The outer radii of the liquid inclusion and coating are R_i and R_c, respectively. The coating and the matrix are assumed to be linear elastic and isotropic with shear modulus G_a (N/m^2) and Poisson ratio ν_a, where $a = c$ for the coating solid and $a = m$ for the matrix. We also assume the initial pressure of the liquid is zero so that the matrix is free of stress before far field loading.

The governing equations in the matrix are:

$$\boldsymbol{\varepsilon}^{(m)} = \frac{1}{2}\left(\nabla \mathbf{u}^{(m)} + \mathbf{u}^{(m)}\nabla\right),$$

$$\boldsymbol{\sigma}^{(m)} = 2G_m\left[\frac{\nu_m}{1-2\nu_m}\mathrm{tr}\left(\boldsymbol{\varepsilon}^{(m)}\right) + \boldsymbol{\varepsilon}^{(m)}\right], \tag{1}$$

$$\nabla \cdot \boldsymbol{\sigma}^{(m)} = 0,$$

where $\mathbf{u}^{(m)}$, $\boldsymbol{\varepsilon}^{(m)}$ and $\boldsymbol{\sigma}^{(m)}$ are the displacement vector, strain tensor, and stress tensor in the matrix, respectively, and G_m (N/m^2) and ν_m are the shear modulus and Poisson ratio of the matrix material, respectively. Those in the coating are

$$\boldsymbol{\varepsilon}^{(c)} = \frac{1}{2}\left(\nabla \mathbf{u}^{(c)} + \mathbf{u}^{(c)}\nabla\right),$$

$$\boldsymbol{\sigma}^{(c)} = 2G_c\left[\frac{\nu_c}{1-2\nu_c}\mathrm{tr}\left(\boldsymbol{\varepsilon}^{(c)}\right) + \boldsymbol{\varepsilon}^{(c)}\right], \tag{2}$$

$$\nabla \cdot \boldsymbol{\sigma}^{(c)} = 0,$$

where $\mathbf{u}^{(c)}$, $\boldsymbol{\varepsilon}^{(c)}$ and $\boldsymbol{\sigma}^{(c)}$ are the displacement vector, strain tensor and stress tensor in the coating, respectively, and G_c (N/m^2)

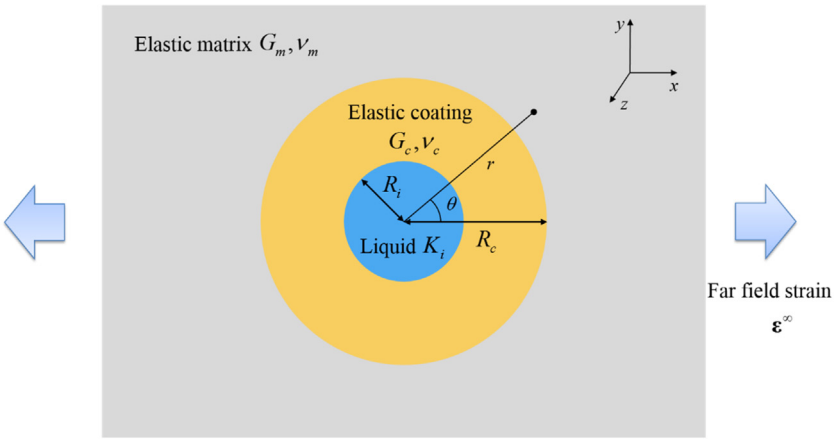

Fig. 2. Mechanical model. We model a spherical liquid inclusion coated with an elastic solid coating embedded in an infinite elastic matrix. The radius of the liquid inclusion is R_i and the radius of the coating is R_c. The inclusion is a liquid with bulk modulus K_i. The coating and the matrix are assumed to be linear elastic and isotropic. Their shear modulus and Poisson's ratio are G_i (N/m^2) and ν_i, where $i = c$ for the coating solid and $i = m$ for the matrix. A uniform far field strain $\boldsymbol{\varepsilon}^{\infty}$ is imposed.

and ν_c are the shear modulus and Poisson ratio of the coating material, respectively.

The liquid is linearly compressible [42]:

$$3K_i \frac{\Delta V}{V} = -p, \tag{3}$$

where K_i (N/m^2) is the bulk modulus of the liquid, V and ΔV are the initial volume and change in volume of the inclusion, respectively, and p is the liquid pressure after loading.

In the far field, a uniform strain $\boldsymbol{\varepsilon}^{\infty}$ is applied

$$\boldsymbol{\varepsilon}^{(m)}\big|_{|\mathbf{x}|\to\infty} = \boldsymbol{\varepsilon}^{\infty}. \tag{4}$$

We focus on the solution for uniaxial loading, so that the far field strain $\boldsymbol{\varepsilon}^{\infty}$ can be written as

$$\boldsymbol{\varepsilon}^{\infty} = \begin{pmatrix} \varepsilon^{\infty} & 0 & 0 \\ 0 & -\nu_m \varepsilon^{\infty} & 0 \\ 0 & 0 & -\nu_m \varepsilon^{\infty} \end{pmatrix}, \tag{5}$$

where $\varepsilon^{\infty} > 0$ represents stretch and $\varepsilon^{\infty} < 0$ represents compression. Note that solutions for simple shear and hydrostatic loading can be derived from this.

At the interface of the liquid inclusion and its coating, force equilibrium requires

$$\boldsymbol{\sigma}^{(c)} \cdot \mathbf{n}_1 = -p\mathbf{n}_1, \tag{6}$$

where $\mathbf{n}_1$ is the normal vector of the liquid-coating interface. Similarly, at the interface of the coating and matrix,

$$\boldsymbol{\sigma}^{(c)} \cdot \mathbf{n}_2 = \boldsymbol{\sigma}^{(m)} \cdot \mathbf{n}_2, \tag{7}$$

where $\mathbf{n}_2$ is the normal vector of the coating-matrix interface. At the interface of the coating and matrix, displacement continuity requires:

$$\mathbf{u}^{(c)} = \mathbf{u}^{(m)}, \tag{8}$$

where $\mathbf{u}^{(c)}$ and $\mathbf{u}^{(m)}$ are the displacement of the coating and matrix, respectively.

3. Solution of the problem

3.1. The elastic fields of a coated liquid inclusion

In a polar coordinate system (Fig. 2), the general solution to the above equations can be written by Legendre polynomial-based solutions:

$$\begin{aligned} u_r &= \sum_{n=0}^{\infty} \left[\frac{A_n}{r^n} n\,(n+3-4\upsilon) - \frac{B_n\,(n+1)}{r^{n+2}} \right] P_n(\cos\theta) \\ &\quad + \sum_{n=-\infty}^{-1} \left[\frac{A_n}{r^n} n\,(n+3-4\upsilon) - \frac{B_n\,(n+1)}{r^{n+2}} \right] P_{-n-1}(\cos\theta), \\ u_\theta &= \sum_{n=0}^{\infty} \left[\frac{A_n}{r^n}(-n+4-4\upsilon) + \frac{B_n}{r^{n+2}} \right] \frac{\partial}{\partial\theta} P_n(\cos\theta) \\ &\quad + \sum_{n=-\infty}^{-1} \left[\frac{A_n}{r^n}(-n+4-4\upsilon) + \frac{B_n}{r^{n+2}} \right] \frac{\partial}{\partial\theta} P_{-n-1}(\cos\theta), \end{aligned} \tag{9}$$

where υ is the Poisson ratio of the coating or matrix and $P_n(\cos\theta)$ is the Legendre polynomial of rank n. Although there are infinite terms in the general solution (9), only a finite number of terms is needed depending upon the boundary conditions. For example, for a coated rigid inclusion problem, only the terms related to $\cos\theta$ and $\sin\theta$ are needed [43]. For the present solution, a radial deformation and a deformation with rotational symmetry with respect to θ are required, so that the displacement fields in the coating and matrix can be expressed as

$$\begin{aligned} u_r^{(a)} &= B_1^{(a)} \varepsilon r + B_2^{(a)} \frac{R_i^3}{r^2} \\ &\quad + \frac{3\cos 2\theta + 1}{4} \left[12\upsilon_i A_1^{(a)} \frac{r^3}{R_i^2} + 2A_2^{(a)} r + 2\,(5-4\upsilon_i) A_3^{(a)} \frac{R_i^3}{r^2} \right. \\ &\quad \left. - 3A_4^{(a)} \frac{R_i^5}{r^4} \right], \\ u_\theta^{(a)} &= -\frac{3\sin 2\theta}{2} \left[(7-4\upsilon_i) A_1^{(a)} \frac{r^3}{R_i^2} + A_2^{(a)} r + 2\,(1-2\upsilon_i) A_3^{(a)} \frac{R_i^3}{r^2} \right. \\ &\quad \left. + A_4^{(a)} \frac{R_i^5}{r^4} \right], \end{aligned} \tag{10}$$

and the corresponding stress fields in the coating and matrix can be expressed as

$$\begin{aligned}
\sigma_{rr}^{(a)} &= 2G_i\left\{B_1^{(a)}\frac{1+\nu_i}{1-2\nu_i}-2B_2^{(a)}\frac{R_i^3}{r^3}\right.\\
&\quad+\frac{3\cos 2\theta+1}{4}\left[-6\nu_i A_1^{(a)}\frac{r^2}{R_i^2}+2A_2^{(a)}-4\left(5-4\nu_i\right)A_3^{(a)}\frac{R_i^3}{r^3}\right.\\
&\quad\left.\left.+12A_4^{(a)}\frac{R_i^5}{r^5}\right]\right\},\\
\sigma_{r\theta}^{(a)} &= -3G_i\sin 2\theta\left[\left(7+2\nu_i\right)A_1^{(a)}\frac{r^2}{R_i^2}+A_2^{(a)}+2\left(1+\nu_i\right)A_3^{(a)}\frac{R_i^3}{r^3}\right.\\
&\quad\left.-4A_4^{(a)}\frac{R_i^5}{r^5}\right],\\
\sigma_{\theta\theta}^{(a)} &= \frac{G_i}{2}\left\{\left[\frac{4(1+\nu_i)}{1-2\nu_i}B_1^{(a)}+\frac{4(1-\nu_i)}{1-2\nu_i}\frac{R_i^2}{r^2}B_2^{(a)}\right]\right.\\
&\quad-6\left[5\nu_i+7\left(2+\nu_i\right)\cos 2\theta\right]A_1^{(a)}\frac{r^2}{R_i^2}\\
&\quad-2\left(-1+3\cos 2\theta\right)A_2^{(a)}\\
&\quad+2\left(1-2\nu_i\right)\left(5+3\cos 2\theta\right)A_3^{(a)}\frac{R_i^3}{r^3}\\
&\quad\left.-\left(3+7\cos 2\theta\right)A_4^{(a)}\frac{R_i^5}{r^5}\right\},
\end{aligned}\tag{11}$$

where $a = c$ for the coating solid and $a = m$ for the matrix. $A_1^{(a)}, A_2^{(a)}, A_3^{(a)}, A_4^{(a)}$ and $B_1^{(a)}, B_2^{(a)}$ are coefficients to be determined from boundary conditions. Values of these coefficients are presented in the Supplementary Material S1.

For verification, we compare our theoretical solution with finite element (FE) results. Details can be found in the Supplementary Material S2.

3.2. Tuning of coating properties to those of an inclusion

Because cell volume influences a range of cell physiological processes [1,44,45], we focus on how volumetric expansion of cells can be controlled by the properties of a pericellular coating. Cell volume changes over the course of cell cycle, increasing during S-phase and decreasing through M-phase [46,47]. At any phase of the cell cycle, rapid volume changes are possible due to osmotic pressure perturbations and transmembrane fluid and ion transport [48]. These volume changes affect protein concentrations and molecular crowding [2,3], and affect cell stiffness [49], folding and transport of proteins [50], and condensation of chromatin [51]. In the following, we focus on the volumetric strain $\Delta V/V$ and pressure change p of the liquid inclusion. The spherical liquid inclusion becomes ellipsoidal in response to far field uniaxial loading. Its linearized volumetric strain can be given by:

$$\begin{aligned}
\frac{1}{\varepsilon^\infty}\frac{\Delta V}{V} &= \frac{1}{\varepsilon^\infty}\frac{1}{4\pi R_i^3/3}\left\{\frac{4\pi}{3}\left[R_i+u_r^{(c)}\left(r=R_i,\theta=0\right)\right]\right.\\
&\quad\times\left[R_i+u_r^{(c)}\left(r=R_i,\theta=\frac{\pi}{2}\right)\right]\\
&\quad\left.\times\left[R_i+u_r^{(c)}\left(r=R_i,\theta=\frac{\pi}{2}\right)\right]-\frac{4\pi R_i^3}{3}\right\}\\
&= \frac{1}{\varepsilon^\infty R_i}\left[u_r^{(c)}\left(r=R_i,\theta=0\right)+u_r^{(c)}\left(r=R_i,\theta=\frac{\pi}{2}\right)\right.\\
&\quad\left.+u_r^{(c)}\left(r=R_i,\theta=\frac{\pi}{2}\right)\right],
\end{aligned}\tag{12}$$

where the first term in braces is the inclusion volume after applying load, and higher order terms are neglected in the derivation of the latter expression.

By substituting the solution (10), we get the volume change of the liquid inclusion:

$$\frac{1}{\varepsilon^\infty}\frac{\Delta V}{V} = \frac{18\alpha^3 G_c G_m(1-\nu_c)(1-\nu_m)}{3\left(4G_m+3K_i\right)G_c\left(1-\nu_c\right)+\left(\alpha^3-1\right)\left(4G_c+3K_i\right)\left[2\left(1-2\nu_c\right)G_m+G_c\left(1+\nu_c\right)\right]},\tag{13}$$

where $\alpha = R_c/R_i$. Because $\frac{1}{\varepsilon^\infty}\frac{\Delta V}{V} > 0$, the volume of the liquid inclusion increases when the far field load is tensile and decreases when the far field load is compressive.

Setting $R_c/R_i = 1$ in Eq. (13) recovers the volume change for the case of no coating reported by Chen et al. [52]:

$$\frac{1}{\varepsilon^\infty}\left(\frac{\Delta V}{V}\right)_0 = \frac{6G_m(1-\nu_m)}{4G_m+3K_i}.\tag{14}$$

The volumetric tuning achieved by a coating can be described by the difference of Eqs. (13) and (14): Eq. (15) which is given in Box I.

A positive difference in Eq. (15) means that the volumetric strain of the inclusion is amplified by the coating, and a negative difference means that the volumetric strain of the inclusion is attenuated by the coating.

To determine the sign of the difference in Eq. (15), we use the bulk modulus of the coating

$$K_c = \frac{2G_c\left(1+\nu_c\right)}{3\left(1-2\nu_c\right)},\tag{16}$$

and rewrite the exp. (15) as Eq. (17) which is given in Box II.

Because the denominator of the right hand side of exp. (17) is positive, the sign of exp. (17) depends on the sign of $G_c - G_m$ and $K_i - K_c$, *i.e.*

$$\frac{1}{\varepsilon^\infty}\frac{\Delta V}{V} - \frac{1}{\varepsilon^\infty}\left(\frac{\Delta V}{V}\right)_0\begin{cases}>0, K_c>K_i, G_c<G_m \text{ or } K_c<K_i, G_c>G_m\\ =0, K_c=K_i \text{ or } G_c=G_m\\ <0, K_c<K_i, G_c<G_m \text{ or } K_c>K_i, G_c>G_m\end{cases}.\tag{18}$$

Let us consider a special case to understand (17) and (18) intuitively, where the coating and matrix have the same Poisson ratio (so that $G_c - G_m$ have the same sign as $K_c - K_m$). If we regard the bulk modulus as material stiffness, the volumetric strain is amplified by the coating when the stiffness increases or decreases monotonically from the matrix to inclusion. However, the mechanical signal is attenuated by the coating when it is either the stiffest or least stiff of the three materials.

The pressure within the liquid inclusion can be written from exps. (3) and (13) as:

$$\frac{p}{G_m\varepsilon^\infty} = -\frac{18\alpha^3 G_c K_i(1-\nu_c)(1-\nu_m)}{3\left(4G_m+3K_i\right)G_c\left(1-\nu_c\right)+\left(\alpha^3-1\right)\left(4G_c+3K_i\right)\left[2\left(1-2\nu_c\right)G_m+G_c\left(1+\nu_c\right)\right]},\tag{19}$$

where $\alpha = R_c/R_i$ is the ratio of the coating radius to the inclusion radius. The negative sign represents that the inclusion pressure decreases when stretch is applied at far field.

For $\alpha = 1$, exp. (19) yields the inclusion pressure for the case of no coating:

$$\frac{p_0}{G_m\varepsilon^\infty} = -\frac{6K_i(1-\nu_m)}{4G_m+3K_i}.\tag{20}$$

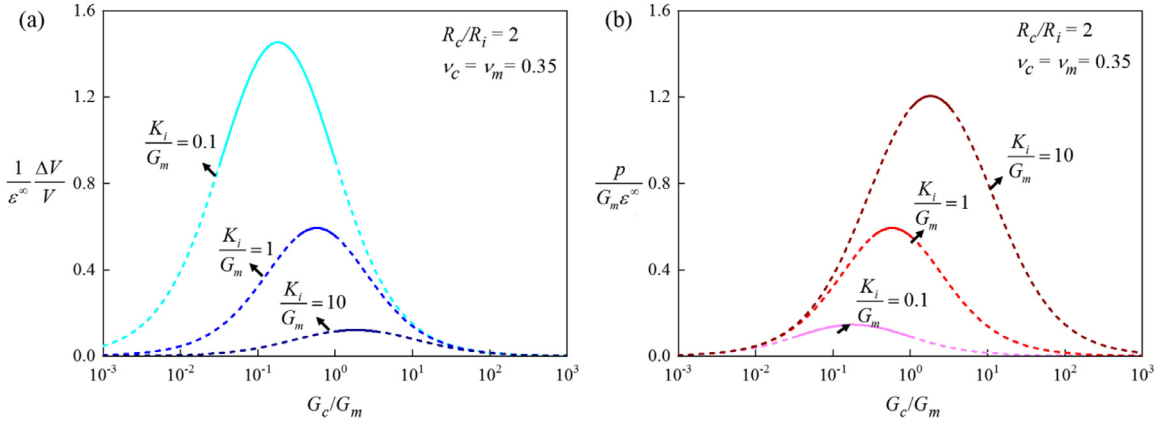

Fig. 3. Tuning of mechanical fields within a coated liquid inclusion embedded in a matrix that is loaded in uniaxial tension. Dashed lines represent attenuation of pressure or dilatation relative to values expected in the absence of a coating; solid lines represent amplification. In these graphs, $\nu_c = 0.35$, $\nu_m = 0.35$ and $\alpha = R_c/R_i = 2$. (a) Dilatation. (b) Hydrostatic pressure.

$$\frac{1}{\varepsilon^\infty}\frac{\Delta V}{V} - \frac{1}{\varepsilon^\infty}\left(\frac{\Delta V}{V}\right)_0 = \frac{12\left(\alpha^3-1\right)(G_c-G_m)\left[3K_i(1-2\nu_c)-2G_c(1+\nu_c)\right]G_m(1-\nu_m)}{(4G_m+3K_i)\left\{3(4G_m+3K_i)G_c(1-\nu_c)+\left(\alpha^3-1\right)(4G_c+3K_i)\left[2(1-2\nu_c)G_m+G_c(1+\nu_c)\right]\right\}}. \tag{15}$$

Box I.

$$\frac{1}{\varepsilon^\infty}\frac{\Delta V}{V} - \frac{1}{\varepsilon^\infty}\left(\frac{\Delta V}{V}\right)_0 = \frac{36\left(\alpha^3-1\right)(G_c-G_m)(K_i-K_c)G_m(1-\nu_m)(1-2\nu_c)}{(4G_m+3K_i)\left\{3(4G_m+3K_i)G_c(1-\nu_c)+\left(\alpha^3-1\right)(4G_c+3K_i)\left[2(1-2\nu_c)G_m+G_c(1+\nu_c)\right]\right\}}. \tag{17}$$

Box II.

$$\frac{|p|-|p_0|}{G_m\varepsilon^\infty} = \frac{36\left(\alpha^3-1\right)(G_c-G_m)(K_i-K_c)K_i(1-\nu_m)(1-2\nu_c)}{(4G_m+3K_i)\left\{3(4G_m+3K_i)G_c(1-\nu_c)+\left(\alpha^3-1\right)(4G_c+3K_i)\left[2(1-2\nu_c)G_m+G_c(1+\nu_c)\right]\right\}}. \tag{21}$$

Box III.

Then, the effect of coating on inclusion pressure can be expressed as Eqs. (21) which is given in Box III.

Obviously,

$$\frac{|p|-|p_0|}{G_m\varepsilon^\infty}\begin{cases} >0, K_c > K_i, G_c < G_m \text{ or } K_c < K_i, G_c > G_m \\ =0, K_c = K_i \text{ or } G_c = G_m \\ <0, K_c < K_i, G_c < G_m \text{ or } K_c > K_i, G_c > G_m \end{cases}. \tag{22}$$

Comparing exps. (18) and (22), we observe that the tuning of pressure by the coating follows the same trends as the tuning of volumetric strain.

4. Results

The dilatation (change in volume per unit initial volume) and hydrostatic pressure within a liquid inclusion can be tuned by altering the mechanical properties and thickness of its coating. These effects are strongly dependent upon the relative mechanical properties of the inclusion, coating, and matrix, but are only weakly dependent upon the Poisson ratios of the coating and matrix. In the examples that follow, we chose $\nu_c = 0.35$ and $\nu_m = 0.35$, which are reasonable for biomaterials and tissues, typically on the order of 0.3–0.5.

The dilatation and hydrostatic pressure in a liquid inclusion subjected to far uniaxial loading can be amplified, or attenuated, by the properties of its coating, as predicted by exp. (13) and exp. (22). As evident in Fig. 3, for $\alpha = R_c/R_i = 2$, these quantities depend upon the relative properties of the inclusion, coating, and matrix. In regions represented by solid lines, the coating amplifies the response of the inclusion relative to the dilatation or hydrostatic pressure that would exist in the absence of a coating; while in regions represented by dashed lines, the coating attenuates these responses. The inclusion dilatation and pressure are attenuated when the shear modulus of the coating is either much greater or smaller than that of the matrix, and amplified when they have similar magnitude.

The dilatation of the liquid inclusion can also be tailored by modulating the coating thickness (Fig. 4, with values of G_c/G_m and K_c/K_i such that all lines satisfy $K_i/G_m = 1$), but only over a limited range of coating thickness. The inclusion is sensitive to the

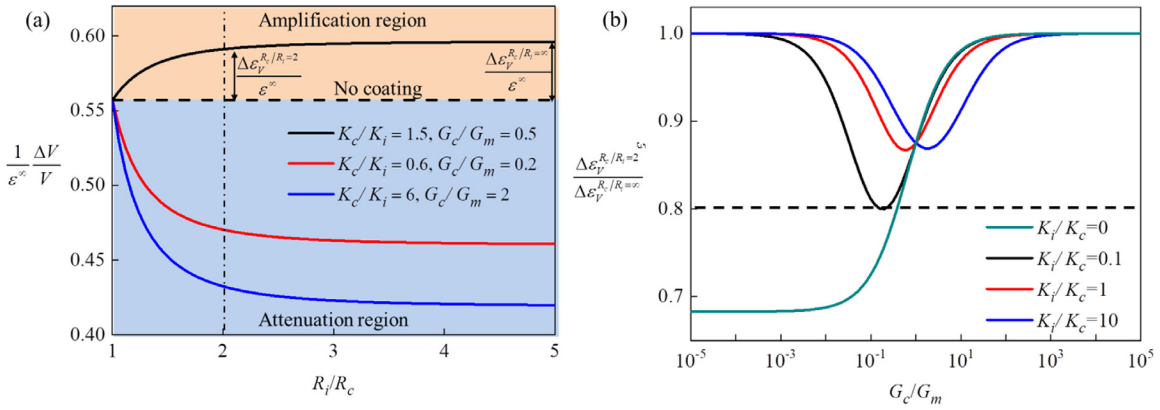

Fig. 4. The effect of coating thickness on the volumetric strain of the inclusion. (a) A coating can enhance the amplification or attenuation of mechanical signals in a fluid filled inclusion. However, the sign of the effect (that is, the amplification or attenuation) depends upon the relative material properties of the inclusion, coating, and matrix. (Dashed line: no coating; upper region: amplification region; lower region: attenuation). Parameters are chosen such that $K_i/G_m = 1$ in this figure. When $R_c/R_i \geq 3$, the effect of coating thickness reaches an asymptote. (b) For $R_c/R_i = 2$, the effect of a coating, as measured by the ratio $\varepsilon_V^{R_c/R_i=2}/\varepsilon_V^{R_c/R_i=\infty}$ (see text) is at least 2/3 of the maximum, regardless of the relative stiffnesses of phases. In these figures, $\nu_c = 0.35$ and $\nu_m = 0.35$.

thickness of the coating for coating thicknesses in the range $1 \leq R_c/R_i \leq 2$, and reaches an asymptote of insensitivity near $R_c/R_i = 3$. Although the coating could affect the degree of attenuation or amplification of dilatation, the sign of the effect (that is whether amplification or attenuation occurs) is determined exclusively by the relative mechanical properties of the coating.

Note that the asymptotic behavior in terms of coating thickness in Fig. 4 (a) does not mean that the matrix properties become irrelevant in the limit of a thick coating. To clarify this, we have

$$\lim_{\alpha\to\infty} \frac{1}{\varepsilon^\infty}\frac{\Delta V}{V} = \frac{18G_cG_m(1-\nu_c)(1-\nu_m)}{(4G_c+3K_i)\left[2\left(1-2\nu_c\right)G_m+G_c\left(1+\nu_c\right)\right]},$$

or

$$\lim_{\alpha\to\infty} \frac{1}{G_m\varepsilon^\infty}\frac{\Delta V}{V} = \frac{18G_c(1-\nu_c)(1-\nu_m)}{(4G_c+3K_i)\left[2\left(1-2\nu_c\right)G_m+G_c\left(1+\nu_c\right)\right]},$$

according to (13). The two expressions above show that the mechanical properties of the matrix are important for the volumetric strain in the thick coating limit, no matter what far field stress or strain is prescribed. The mechanism for this is intuitive: the force acting on the coating-matrix boundary, which will affect the volumetric strain of the inclusion, depends on both the coating and the matrix, regardless of the far field stress or strain that is prescribed.

To explore sensitivity to coating thickness, we studied the case of the coating thickness equaling the coating radius ($R_c/R_i = 2$) and explored the ratio $\Delta\varepsilon_V^\alpha/\Delta\varepsilon_V^\infty$, where $\Delta\varepsilon_V^\alpha$ is defined as

$$\Delta\varepsilon_V^{R_c/R_i} = \frac{\Delta V\left(R_c/R_i\right)}{V} - \left(\frac{\Delta V}{V}\right)_0, \tag{23}$$

and $\Delta\varepsilon_V^{\alpha=\infty}$ is defined as

$$\Delta\varepsilon_V^{\alpha=\infty} = \frac{\Delta V\left(R_c/R_i=\infty\right)}{V} - \left(\frac{\Delta V}{V}\right)_0, \tag{24}$$

We represent the $\Delta\varepsilon_V^\alpha$ and $\Delta\varepsilon_V^\infty$ in Fig. 4(a). We plot $\Delta\varepsilon_V^{\alpha=2}/\Delta\varepsilon_V^\infty$ in Fig. 4(b) for several values of K_i/G_m. All lines pass through the same point when $G_c/G_m = 1$, which means that the coating material is the same as the matrix. The coating effect is at least 2/3 of the maximum when $R_c/R_i = 2$, independent of the coating stiffness. Results are similar for the influence of coating thickness on hydrostatic pressure (see Supplementary material S3).

5. Mechanism of mechanical tuning by coating

5.1. Radial stress transmission through the coating

To simplify the solution, we used superposition to replicate a uniaxial load, and noted that in simple shear, which can be represented by orthogonal stretch and compression, the inclusion volume does not change:

$$\boldsymbol{\sigma}^\infty = \begin{pmatrix}\sigma^\infty & 0 & 0\\ 0 & 0 & 0\\ 0 & 0 & 0\end{pmatrix} = \begin{pmatrix}\frac{\sigma^\infty}{3} & 0 & 0\\ 0 & \frac{\sigma^\infty}{3} & 0\\ 0 & 0 & \frac{\sigma^\infty}{3}\end{pmatrix} + \begin{pmatrix}\frac{\sigma^\infty}{3} & 0 & 0\\ 0 & -\frac{\sigma^\infty}{3} & 0\\ 0 & 0 & 0\end{pmatrix} + \begin{pmatrix}\frac{\sigma^\infty}{3} & 0 & 0\\ 0 & 0 & 0\\ 0 & 0 & -\frac{\sigma^\infty}{3}\end{pmatrix} \tag{25}$$

where the latter two terms represent simple shear. Considering that simple shear does not change the inclusion volume, the volumetric strain of the inclusion is induced by the radial component in the far field load, *i.e.*, the first term in Eq. (25). The volumetric strain arising from a uniaxial loading is thus the same as that arising from a uniform radial load. The elastic fields of the problem under radial load are shown in the Supplementary Material S4, which are superposed by elastic fields derived in (10) and (11) and are analogous to those in Saadat et al. [6].

From Eqs. (18) and (22) we observe that the coating effect on the inclusion volumetric strain vanishes when either $K_i = K_c$ or $G_c = G_m$. We will first explain these critical cases. For the case of $K_i = K_c$, the inclusion and coating have the same compressibility and behave like an inclusion with radius R_c and bulk modulus K_c when uniform radial load is applied. The elastic fields for this case (Supplementary Material S4) also show this: the stress field in the coating is uniform and the same as the inclusion. For $G_c = G_m$, the coating effect vanishes because, as derived in Supplementary Material S4, the elastic fields in the coating and inclusion are independent of coating thickness R_c/R_i, including $R_c/R_i = 0$.

To explore how dilatation and pressure depend on material properties in the solution of Supplementary Material S4, we again explored the case of $\nu_c = 0.35$ and $\nu_m = 0.35$ and studied a range of coating shear moduli.

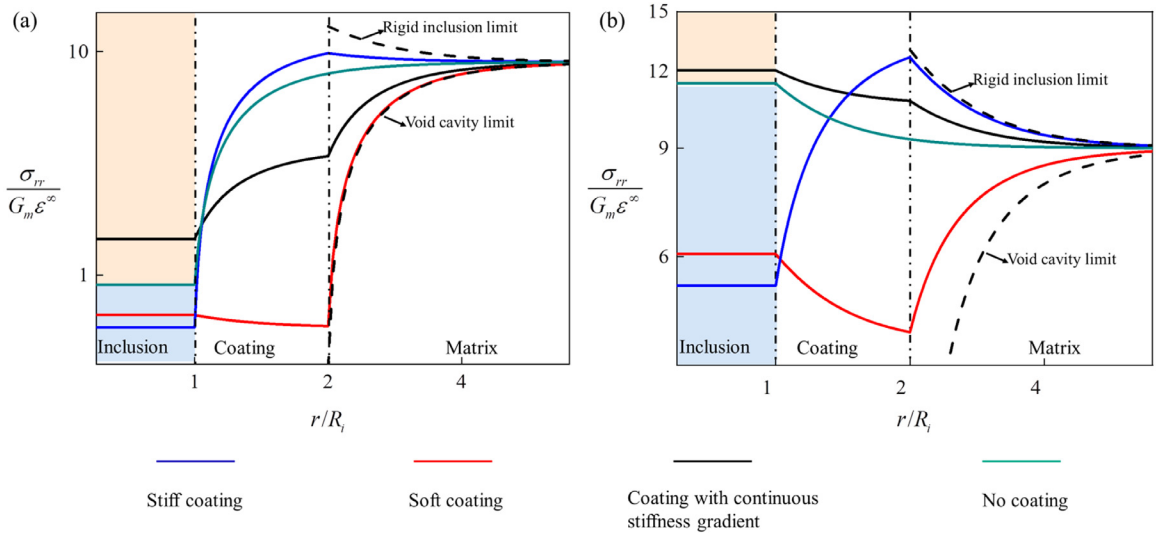

Fig. 5. Investigation of the coating effects on the inclusion pressure. The inclusion pressure depends on the transmission of radial stress through the coating ((a) and (b)). (a) represents the case of $K_i/G_m = 0.1$, and (b) represents the case of $K_i/G_m = 10$. In these figures, we fix the Poisson ratio of the coating and matrix, $\nu_c = 0.35$ and $\nu_m = 0.35$. The blue lines represent the cases of stiff coating (*i.e.* $K_c/K_i = 60$, $G_c/G_m = 2$ in (a), $K_c/K_i = 6$, $G_c/G_m = 20$ in (b)). The red lines represent the cases of soft coating (i.e. $K_c/K_i = 0.6$, $G_c/G_m = 0.02$ in (a), $K_c/K_i = 0.06$, $G_c/G_m = 0.2$ in (b)). The black lines represent the cases of the coating with amplification effect (i.e. $K_c/K_i = 6$, $G_c/G_m = 0.2$ in (a), $K_c/K_i = 0.6$, $G_c/G_m = 2$ in (b)). Green lines represent the case of no coating. According to the value of the green lines in the inclusion (i.e. $r/R_i \leq 1$), we divide two regions. The region above the green line is the amplification region and the region below the green line is the attenuation region. . (For interpretation of the references to color in this figure legend, the reader is referred to the web version of this article.)

According to the solution in Supplementary Material S4, we plot the radial stress in the inclusion, coating and matrix in Fig. 5(a) for $K_i/G_m = 0.1$ and (b) for $K_i/G_m = 10$. In these figures, the blue lines represent the cases of a stiff coating (*i.e.* $K_c/K_i = 60$, $G_c/G_m = 2$ in (a), and $K_c/K_i = 6$, $G_c/G_m = 20$ in (b)). The red lines represent the cases of a soft coating (*i.e.* $K_c/K_i = 0.6$, $G_c/G_m = 0.02$ in (a), and $K_c/K_i = 0.06$, $G_c/G_m = 0.2$ in (b)). The black lines represent the cases of the coating with amplification effect (*i.e.* $K_c/K_i = 6$, $G_c/G_m = 0.2$ in (a), and $K_c/K_i = 0.6$, $G_c/G_m = 2$ in (b)). Green lines represent the case of no coating. According to the value of the green lines in the inclusion (i.e. $r/R_i \leq 1$), two regions emerge. The region above the green line is the amplification region and the region below the green line is the attenuation region. The dashed lines represent the limiting cases of a rigid coating and a cavity.

For the case of a stiff inclusion, the radial stress increases rapidly in the matrix, but decays rapidly in the coating (in the direction from the matrix to the inclusion). For the case of soft inclusion, the radial stress decays rapidly in the matrix, and increases slightly in the coating (in the direction from the matrix to the inclusion). Cases of both stiff and soft coatings fall in the attenuation region. However, for the case of a coating with amplification effect, the radial stress changes monotonously from the far field to the inclusion. This case falls in the amplification region.

5.2. Tuning mechanisms

Inspired by the radial stress transmission from the far field to the inclusion (Fig. 5), we present an intuitive physical explanation for the attenuation and amplification effects of coating. In this part, we only state intuitive views. Whether these intuitive views are correct can be justified by the solution in the Supplementary Material S4. We note that although the explanation is for extreme situations, it at least provides us with an intuitive view of the attenuation and amplification effects of the coating.

We begin with a basic lemma that can be established with a thought experiment for a non-coated liquid inclusion embedded in a radially loaded infinite or finite solid (Fig. 6(a–b)): the pressure p^i within the inclusion will differ from the applied radial far-field or boundary load, p_{load}, by an amount:

$$p^i - p_{load} \begin{cases} > 0, K_i > K_s \\ = 0, K_i = K_s \\ < 0, K_i < K_s \end{cases} \tag{26}$$

with $\left|p^i - p_{load}\right|$ increasing with $|K_i - K_s|$. The argument is clear by first considering the limiting case of a compliant inclusion, with properties approaching those of a void ($K_i \ll K_s$). Because the void cannot bear a load, the pressure in the inclusion will be small compared to the remote pressure, and $p^i < p^\infty$. For the case of a relatively rigid inclusion ($K_s \ll K_i$), which means that the liquid deforms less under pressure loading than the solid, an extra pressure is needed to restrain the frustrated dilatation of the solid, and $p^i > p^\infty$. For the case of the liquid having the same bulk modulus as the solid, the two will have same volumetric strain under a radial load and will experience a uniform stress field, $p^i = p^\infty$. This is evident from the green lines representing the case of no coating in Fig. 5).

To extend this to understand the mechanics of a coated liquid inclusion, we provide insight into attenuation and amplification of pressure and dilatation by a coating surrounding an inclusion (Fig. 6(c)). We first consider the case of $G_c < G_m$. In the limit of G_c so small that the coating can be treated as liquid (Fig. 6(d)), the problem becomes one of two liquids, with bulk moduliK_i and K_c, within an elastic solid. In this case, the effective bulk modulus K_{ci} of the composite liquid inclusion satisfies:

$$K_{ci} \begin{cases} > K_i, K_c > K_i \\ = K_i, K_c = K_i \\ < K_i, K_c < K_i \end{cases}. \tag{27}$$

The reference case is the problem that a liquid inclusion with bulk modulus K_i embedded in the matrix. If same radial load p^∞ is applied to the limit case and reference case (Fig. 6(d)), we assume the inclusion pressure in the limit case to be p^i and in the reference state to be p_0^i. We compare p^i and p_0^i to evaluate

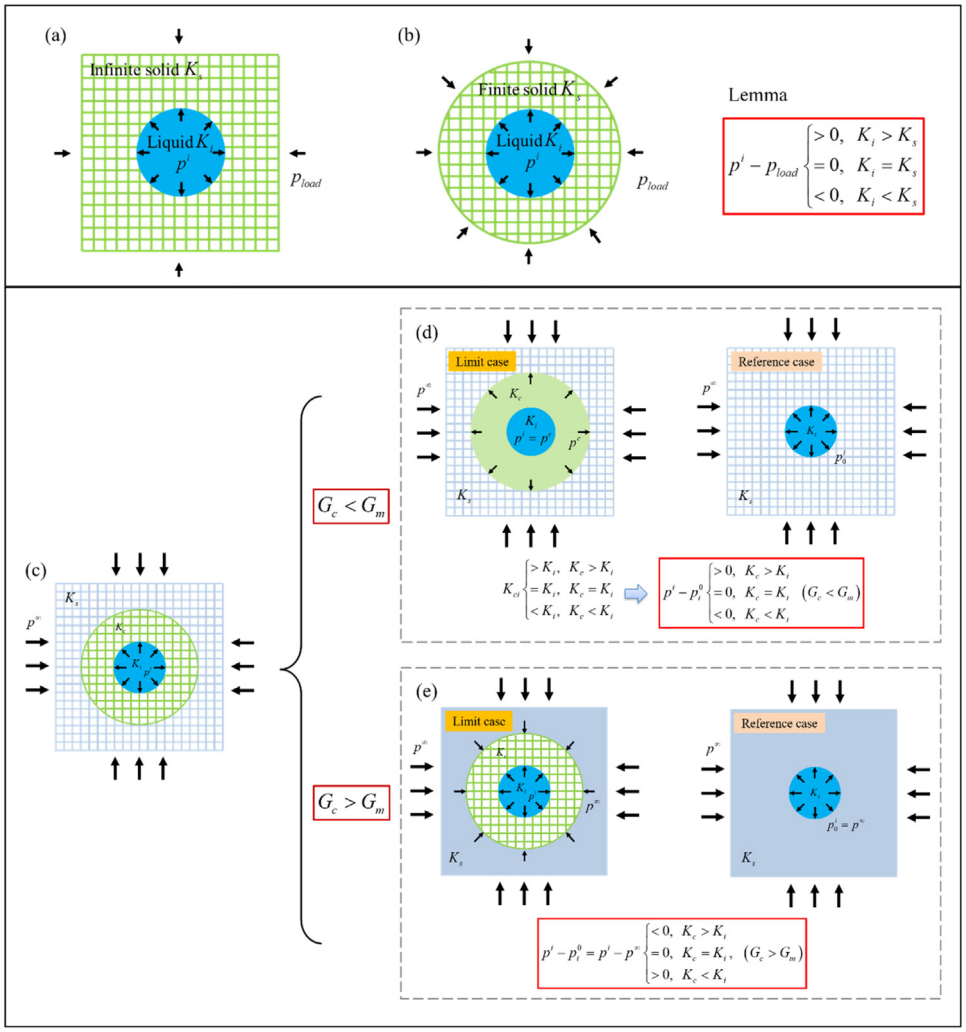

Fig. 6. Schematic of an intuitive explanation of how tuning can be achieved by a coating. A liquid inclusion with bulk modulus K_i embedded in an infinite (a) or finite solid (b) with bulk modulus K_s. Radial stress p_{load} is applied on the boundary of the solid, which induces a liquid pressure p^i. The difference between p^i and p_{load} depends on the relative value of K_i and K_s. Based on this property as a lemma, we give an intuitive explanation of the amplification and attenuation effect of the coating for some limit cases. The case to be explained is shown in (c). (d) is the limit case for $G_c < G_m$, *i.e.* G_c is so small to be considered as a liquid. (e) is the limit case for $G_c > G_m$, *i.e.* G_m is so small to be considered as a liquid. The tuning role in limit cases (d) and (e) is intuitive based on the lemma shown in (a) and (b). In these figures, the meshed parts represent solids and unmeshed parts represent liquids.

the coating effect. We should note that p^i is also the pressure of the liquid composite, because the pressure is uniform in a liquid composite. According to the **Lemma** stated above, $p^i > p_0^i$ if the effective bulk modulus K_{ci} of the mixture is greater than the bulk modulus K_i of the inclusion, $p^i = p_0^i$ if the effective bulk modulus K_{ci} of the composite equals to the bulk modulus K_i of the inclusion, and $p^i < p_0^i$ if the effective bulk modulus K_{ci} of the composite is smaller than the bulk modulus K_i of the inclusion. According to (27), we have

$$p^i - p_i^0 \begin{cases} > 0, K_c > K_i \\ = 0, K_c = K_i \ (\text{if}\, G_c < G_m)\,. \\ < 0, K_c < K_i \end{cases} \tag{28}$$

This expression gives an intuitive view of coating effects for the case of $G_c < G_m$.

We then consider the case of $G_c > G_m$. For G_m so small that the matrix can be treated as a liquid (Fig. 6(e)), the reference state is the problem of a liquid inclusion with bulk modulus K_i embedded in a liquid matrix. If same radial load p^∞ is applied to the limit case and reference case, we assume the inclusion pressure in the limit case to be p^i and in the reference state to be p_0^i. We again compare p^i and p_0^i to evaluate the effect of the coating. Because the matrix can be treated as a liquid, the load applied on the coating by the matrix is p^∞. According to the lemma, we have

$$p^i - p^\infty \begin{cases} < 0, K_c > K_i \\ = 0, K_c = K_i\ , (G_c > G_m) \\ > 0, K_c < K_i \end{cases} \tag{29}$$

for the limit case. We should also note that $p_0^i = p^\infty$, because the pressure is uniform in liquid. Then we have the comparison between p^i and p^∞:

$$p^i - p_i^0 = p^i - p^\infty \begin{cases} < 0, K_c > K_i \\ = 0, K_c = K_i\ , \quad (G_c > G_m) \\ > 0, K_c < K_i \end{cases} \tag{30}$$

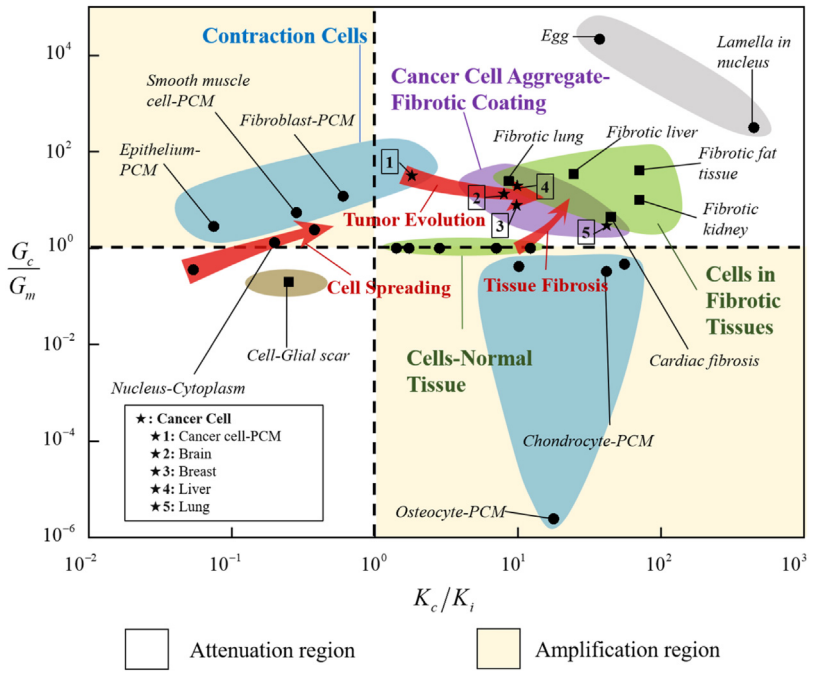

Fig. 7. Examples of coated inclusions. A coating can amplify or attenuate dilatation experienced by a fluid-filled inclusion. Data (cf. Table S1) interpreted through our model suggest that amplification can switch to attenuation in certain pathologies. The first and third quadrants represent attenuation, and the second and fourth represent amplification.

This expression gives an intuitive view of coating effects for the case of $G_c > G_m$.

6. Application to coated inclusions in physiology and nature

To explore the entire range of situations expected in biological applications, we explored distributions of coated liquid inclusions ranging from sparse cells, to cell aggregates, to organelles within a homogenized cell (Supplementary Material S5). For cell aggregates, the mechanical fields from neighboring cells can be expected to interact. There is a rich history in the field of homogenization theory in addressing these interactions, including the self-consistent method from micromechanics [53], wherein the mechanical properties of the matrix are chosen to represent the effects of neighboring cells. Note that according to the results of Section 5.1, the volumetric strain of the inclusion is induced by the radial component in the far field load, no matter the inclusion is liquid or solid, and that according to the results of the Supplementary Material S5, the solution for dilatation of solid and liquid inclusions under radial load are identical, and amplification or attenuation of volumetric strain is qualitatively determined by the sign of $(G_c - G_m)$ $(K_i - K_c)$ in both cases, regardless of Poisson ratios of coating and matrix. In this section, we use this rule to understand coated inclusions in nature, with K_c/K_i and G_c/G_m estimated as in Table S1 (Fig. 7). With the plane of $(K_c/K_i, G_c/G_m)$ divided into four quadrants, quadrants I and III represent conditions of attenuation, and quadrants II and IV represent conditions of amplification region.

At the cellular length scale, we begin by considering cells in connective tissues such as bone, tendon, and cartilage. Tendon and bone are stiff ($G > 100$ kPa) compared to the cells that they contain, which leads to an interesting puzzle: *in vitro*, the mechanosensitive osteocytes that are critical to bone homeostasis show responses to strains greater than 5×10^{-3}, but these levels exceed injury thresholds in bone ($\sim 3.5 \times 10^{-3}$) [54]. However, osteocytes are surrounded by a coating of pericellular matrix (PCM) with bulk modulus greater than that of the cells themselves, and with shear modulus smaller than that of the matrix [54]. In this case, the placement of osteocytes on Fig. 7 shows that the PCM amplifies mechanical signals. Similar results occur for PCM surrounding the chondrocyte cells in cartilage (Fig. 7; see also [6,55]. In both cases, volumetric strain is amplified by the PCM.

A number of cells remodel their ECM [56], and can further stiffen their environment by contraction [13,57]. These cells thereby form a PCM coating. Plotting K_c/K_i and G_c/G_m for a range of cells (Fig. 7) reveals that certain cancerous cell ("1" in Fig. 7) differ from fibroblasts, smooth muscle cells, and epithelial cells: cancer cell PCM attenuates volumetric strain, while those of their healthy counterparts amplify volumetric strain. Many cancer cell aggregates are surrounded by collagen coatings, the bulk modulus and shear modulus of which can be greater than those of the cancer cell aggregates and matrix (Table S1). On Fig. 7 (numbers "2" -"5"), the evolution from cancer cell to tumor evolution appears as a process of further attenuation of volumetric strain of its inclusion, rather like an egg shell insulates an embryo (Fig. 7), further insulating the cells within the aggregate from physiological signaling.

Another pathology characterized by our model as progressive and maladaptive changes to mechanosensation is fibrosis, *i.e.*, the formation of excess fibrous connective tissue that is stiffer than healthy tissues and cells (Table S1). Fibrosis can arise from scarring and from diseases such as hepatitis C, hypertension, and chronic inflammation [58–60]. Remodeling of ECM and synthesis of excess ECM proteins occurs in the direct vicinity of fibroblasts [61,62], and we therefore treat fibroblasts as coated inclusions. In the context of our visualization in Fig. 7, fibrosis upsets a delicate balance and causes a shift of tissue properties to the quadrant in which attenuation occurs. Fibrosis thus attenuates mechanical signals sensed by fibroblasts.

Glial scars represent another case of formation of a coating surrounding a cell, this time in the central nervous system [63,

64]. These coatings arise following injury and interfere with healing. According to our model, they also attenuate deformation of neurons (Fig. 7), consistent with the observation of Moeendarbary et al. that neural regeneration is inhibited by the increasing mismatch between stiff glial scars and the tissues of the central nervous system, which become more compliant following injury [64].

The model can also be applied to organelles within cells, again considering cells that are rounded in the early stages of exposure to ECM, or that are constitutively round such as chondrocytes within cartilage. The nucleus of a cell is connected to the ECM by proteins called the LINC complex that connect to the cytoskeleton [65]. The nuclear membrane is coated by laminas that can be elastic or viscoelastic, and that can remodel in response to the cell microenvironment and pathology [66–68]. A central question in mechanobiology is how the nucleus senses external mechanical signals [69,70]. The whole nucleus (including laminated nuclear envelope and nucleoplasm) is 5–10 times stiffer than the cytoplasm, and the laminated nuclear envelope has a thickness that is about 10% the radius of the nucleus [71,72]. Upon treating the cytoplasm as a coating around the nucleus and estimating $K_c/K_i = 2.00 \times 10^2 \sim 1.00 \times 10^3$ and $G_c/G_m = 2,00 \times 10^2 \sim 5.00 \times 10^2$, Fig. 7 suggests that the lamina insulates the nucleus from large deformation. This however changes over cell spreading. Cytoplasm is more compliant than both the nucleus and ECM in an unspread cell, but develops a stiffness between that of the nucleus and ECM during cell spreading [16,73]. Plotting this process on Fig. 7 suggests that cell spreading thus enables the nuclei to increasingly "feel" their microenvironments.

Modulating cell volume further enables cells to modulate this mechanosensitivity. The sensitivity to coating size drops dramatically for $R_c/R_i \geq 2$ and reaches at least 2/3 of the maximum when $R_c/R_i = 2$, no matter the stiffness of the coating. In other words, $R_c/R_i = 2$ is a cell size that enables tuned pressure transmission to the nucleus, but at a minimum of volume. This corresponds to a cell nucleus that is about 10% of the volume of a suspended, unspread cell, which is a characteristic value.

7. Conclusions

Our analytical model of the mechanics of a coated liquid inclusion identified a key quantity that determines whether dilatation is amplified or attenuated by a coating: if $(G_c - G_m)(K_i - K_c) > 0$, the coating amplifies dilatation of the inclusion; if $(G_c - G_m)(K_i - K_c) < 0$, the coating attenuates dilatation. The thickness of the coating can accentuate the effect of the coating, but not change the effect from amplification to attenuation, and the effect reaches an asymptote for coatings of thickness more than three times the radius of the inclusion.

When studied in the context of our model, data suggested that cells, cell aggregates, and subcellular organelles can tune the mechanical stimuli that they experience by remodeling the coatings surrounding them. At the level of subcellular organelles, the nuclear lamina may serve as a coating that either insulates the nucleus, or, in the case of a 10% nucleus-to-cytoplasm ratio in the early stages of cell spreading, might amplify mechanical cues. In healthy cells, these coatings are typically tuned to amplify volumetric strains; in pathologies including fibrosis and certain cancers, the coatings that develop around cells and cell aggregates serve to insulate cells from the mechanical stimuli in their environment. Results suggest pathways by which these cells might insulate themselves from mechanobiological cues that could reverse their pathological course, and motivate further study of the role of pericellular matrix in the development of pathology.

Declaration of competing interest

The authors declare that they have no known competing financial interests or personal relationships that could have appeared to influence the work reported in this paper.

Acknowledgments

This work was supported by the National Natural Science Foundation of China (11532009, 11902155, 11972280, 12032010), the Open Fund of the State Key Laboratory of Mechanics and Control of Mechanical Structures (MCMS-I-0219K01 and MCMS-E-0219K02), the Natural Science Foundation of Jiangsu Province (BK20190382), the foundation of "Jiangsu Provincial Key Laboratory of Bionic Functional Materials", the Foundation for the Priority Academic Program Development of Jiangsu Higher Education Institutions, the New Faculty Foundation of NUAA, and the US NSF (CMMI 1548571).

Appendix A. Supplementary materials

Supplementary material related to this article can be found online at https://doi.org/10.1016/j.eml.2020.101049.

References

[1] M. Guo, et al., Cell volume change through water efflux impacts cell stiffness and stem cell fate, Proc. Natl. Acad. Sci. USA 114 (41) (2017) 201705179.
[2] R.J. Ellis, Macromolecular crowding: obvious but underappreciated, Trends Biochem. Sci. 26 (10) (2001) 597–604.
[3] A.P. Minton, The influence of macromolecular crowding and macromolecular confinement on biochemical reactions in physiological media, J. Biol. Chem. 276 (14) (2001) 10577.
[4] H. Lee, et al., Mechanical confinement regulates cartilage matrix formation by chondrocytes, Nature Mater. 16 (12) (2017) 1243.
[5] N. Huebsch, et al., Harnessing traction-mediated manipulation of the cell–matrix interface to control stem cell fate, Nat. Mater. 9 (6) (2010) 518.
[6] F. Saadat, et al., Functional grading of pericellular matrix surrounding chondrocytes: potential roles in signaling and fluid transport, 2018, 365569, bioRxiv.
[7] A. Iordan, et al., Breakdown of cell-collagen networks through collagen remodeling, Biorheology 47 (5–6) (2010) 277–295.
[8] Y.L. Yang, L.M. Leone, L.J. Kaufman, Elastic moduli of collagen gels can be predicted from two-dimensional confocal microscopy, Biophys. J. 97 (7) (2009) 2051–2060.
[9] M. Keating, et al., Spatial distributions of pericellular stiffness in natural extracellular matrices are dependent on cell-mediated proteolysis and contractility, Acta Biomater. 57 (2017) S174270611730291X.
[10] Y.L. Han, et al., Cell contraction induces long-ranged stress stiffening in the extracellular matrix, Proc. Natl. Acad. Sci. USA 115 (16) (2018) 201722619.
[11] B. Babaei, et al., Remodeling by fibroblasts alters the rate-dependent mechanical properties of collagen, Acta Biomater. 37 (2016) 28–37.
[12] A. Abhilash, et al., Remodeling of fibrous extracellular matrices by contractile cells: predictions from discrete fiber network simulations, Biophys. J. 107 (8) (2014) 1829–1840.
[13] M.S. Hall, et al., Fibrous nonlinear elasticity enables positive mechanical feedback between cells and ECMs, Proc. Natl. Acad. Sci. USA 113 (49) (2016) 14043.
[14] K.R. Levental, et al., Matrix crosslinking forces tumor progression by enhancing integrin signaling, Cell 139 (5) (2009) 891–906.
[15] H. Yu, J.K. Mouw, V.M. Weaver, Forcing form and function: biomechanical regulation of tumor evolution, Trends Cell Biol. 21 (1) (2011) 47–56.
[16] J. Chen, et al., Cell mechanics, structure, and function are regulated by the stiffness of the three-dimensional microenvironment, Biophys. J. 103 (6) (2012) 1188–1197.
[17] L.J. Walpole, A coated inclusion in an elastic medium, Math. Proc. Camb. Phil. Soc. 83 (3) (1978) 495–506.
[18] K. Jayaraman, K.L. Reifsnider, Residual stresses in a composite with continuously varying Young's modulus in the fiber/matrix interphase, J. Compos. Mater. 26 (6) (1992) 770–791.
[19] G. Vörös, B. Pukánszky, Effect of a soft interlayer with changing properties on the stress distribution around inclusions and yielding of composites, Composites Part A 32 (3) (2001) 343–352.

[20] H.L. Duan, et al., Stress fields of a spheroidal inhomogeneity with an interphase in an infinite medium under remote loadings, Proc. R. Soc. A Math. Phys. Eng. Sci. 461 (2056) (2005) 1055–1080.
[21] K. Bertoldi, D. Bigoni, W.J. Drugan, Structural interfaces in linear elasticity, part ii: effective properties and neutrality, J. Mech. Phys. Solids 55 (1) (2007) 35–63.
[22] M.W. Yi, et al., Effective moduli of particle-filled composite with inhomogeneous interphase: Part I – bounds, Composites Sci. Technol. 64 (9) (2004) 1345–1351.
[23] Z. Yan, et al., Effective moduli of particle-filled composite with inhomogeneous interphase: Part II – mapping method and evaluation, Composites Sci. Technol. 64 (9) (2004) 1353–1362.
[24] Z. Hashin, Thin interphase/imperfect interface in elasticity with application to coated fiber composites, J. Mech. Phys. Solids 50 (12) (2002) 2509–2537.
[25] S.L. Bai, et al., Microstructures and mechanical properties of polypropylene/polyamide 6/polyethelene-octene elastomer blends, Polymer 45 (9) (2004) 3063–3071.
[26] M. Ostoja-Starzewski, et al., Composites with functionally graded interphases: Mesocontinuum concept and effective transverse conductivity, Acta Mater. 44 (5) (1996) 2057–2066.
[27] W. Wang, I. Jasiuk, Effective elastic constants of particulate composites with inhomogeneous interphases, J. Compos. Mater. 32 (15) (1998) 1391–1424.
[28] R.M. Christensen, K.H. Lo, Solutions for effective shear properties in three phase sphere and cylinder models, J. Mech. Phys. Solids 27 (4) (1979) 315–330.
[29] H.L. Duan, et al., Size-dependent effective elastic constants of solids containing nano-inhomogeneities with interface stress, J. Mech. Phys. Solids 53 (7) (2005) 1574–1596.
[30] B. Jiang, G.J. Weng, A generalized self-consistent polycrystal model for the yield strength of nanocrystalline materials, J. Mech. Phys. Solids 52 (5) (2004) 1125–1149.
[31] Q.S. Zheng, D.X. Du, An explicit and universally applicable estimate for the effective properties of multiphase composites which accounts for inclusion distribution, J. Mech. Phys. Solids 49 (11) (2001) 2765–2788.
[32] M.J. Pablo, G.M. Genin, E.L. Elson, On the application of strain factors for approximation of the contribution of anisotropic cells to the mechanics of a tissue construct, J. Biomech. 39 (11) (2006) 2145.
[33] J.P. Marquez, et al., Thin bio-artificial tissues in plane stress: the relationship between cell and tissue strain, and an improved constitutive model, Biophys. J. 88 (2) (2005) 765–777.
[34] J.P. Marquez, et al., The relationship between cell and tissue strain in three-dimensional bio-artificial tissues, Biophys. J. 88 (2) (2005) 778–789.
[35] C. Chen, et al., Fluidization and resolidification of the human bladder smooth muscle cell in response to transient stretch, PLoS One 5 (8) (2010) e12035.
[36] R. Krishnan, et al., Reinforcement versus fluidization in cytoskeletal mechanoresponsiveness, PLoS One 4 (5) (2009) e5486.
[37] A. Nekouzadeh, et al., Stretch-activated force shedding, force recovery, and cytoskeletal remodeling in contractile fibroblasts, J. Biomech. 41 (14) (2008) 2964–2971.
[38] S.L. Lee, et al., Physically-induced cytoskeleton remodeling of cells in three-dimensional culture, PLoS One 7 (12) (2012) e45512.
[39] R. Kaunas, H.J. Hsu, A kinematic model of stretch-induced stress fiber turnover and reorientation, J. Theoret. Biol. 257 (2) (2009) 320–330.
[40] S. Thomopoulos, et al., Fibrocartilage tissue engineering: The role of the stress environment on cell morphology and matrix expression, Tissue Eng. Part A 17 (7–8) (2011) 1039–1053.
[41] F. Guilak, A. Ratcliffe, V.C. Mow, Chondrocyte deformation and local tissue strain in articular cartilage: a confocal microscopy study, J. Orthop. Res. 13 (3) (1995) 410–421.
[42] B. Shafiro, M. Kachanov, Materials with fluid-filled pores of various shapes: Effective elastic properties and fluid pressure polarization, Int. J. Solids Struct. 34 (27) (1997) 3517–3540.
[43] X. Chen, et al., Translation of a coated rigid spherical inclusion in an elastic matrix: exact solution, and implications for mechanobiology, J. Appl. Mech. 86 (5) (2019) 051002.
[44] E.K. Hoffmann, I.H. Lambert, S.F. Pedersen, Physiology of cell volume regulation in vertebrates, Physiol. Rev. 89 (1) (2009) 193–277.
[45] F. Lang, et al., Functional significance of cell volume regulatory mechanisms, Physiol. Rev. 78 (1) (1998) 247.
[46] T. Amit, et al., Cell growth and size homeostasis in proliferating animal cells, Science 325 (5937) (2009) 167–171.
[47] E. Delpire, K.B. Gagnon, Water homeostasis and cell volume maintenance and regulation, in: Current Topics in Membranes, Elsevier, 2018, pp. 3–52.
[48] T.H. Hui, et al., Volumetric deformation of live cells induced by pressure-activated cross-membrane ion transport, Phys. Rev. Lett. 113 (11) (2014) 118101.
[49] E.H. Zhou, et al., Universal behavior of the osmotically compressed cell and its analogy to the colloidal glass transition, Proc. Natl. Acad. Sci. USA 106 (26) (2009) 10632–10637.
[50] D. Oh, et al., Development of time-integrated multipoint moment analysis for spatially resolved fluctuation spectroscopy with high time resolution, Biophys. J. 101 (6) (2011) 1546–1554.
[51] I. Jerome, et al., Osmotic challenge drives rapid and reversible chromatin condensation in chondrocytes, Biophys. J. 104 (4) (2013) 759–769.
[52] X. Chen, et al., The elastic fields of a compressible liquid inclusion, Extreme Mech. Lett. (2018).
[53] S. Nemat-Nasser, M. Hori, Micromechanics: Overall Properties of Heterogeneous Materials, Vol. 37, Elsevier, 2013.
[54] S.W. Verbruggen, T.J. Vaughan, L.M. Mcnamara, Strain amplification in bone mechanobiology: a computational investigation of the in vivo mechanics of osteocytes, J. R. Soc. Interface 9 (75) (2012) 2735–2744.
[55] H. Sang-Kuy, F. Salvatore, H. Walter, A depth-dependent model of the pericellular microenvironment of chondrocytes in articular cartilage, Comput. Methods Biomech. Biomed. Eng. 14 (7) (2011) 657–664.
[56] L. Albert James, et al., Stress controls the mechanics of collagen networks, Proc. Natl. Acad. Sci. USA 112 (31) (2015) 9573–9578.
[57] S. Yair, S.A. Safran, Scaling laws for the response of nonlinear elastic media with implications for cell mechanics, Phys. Rev. Lett. 108 (17) (2012) 178103.
[58] T. Poynard, P. Bedossa, P. Opolon, Natural history of liver fibrosis progression in patients with chronic hepatitis c, Lancet 349 (9055) (1997) 825–832.
[59] P. Kong, P. Christia, N.G. Frangogiannis, The pathogenesis of cardiac fibrosis, Cell. Mol. Life Sci. 71 (4) (2014) 549–574.
[60] R.M. Strieter, B. Mehrad, New mechanisms of pulmonary fibrosis, Chest 136 (5) (2009) 1364–1370.
[61] G. Raeber, M. Lutolf, J. Hubbell, Mechanisms of 3-d migration and matrix remodeling of fibroblasts within artificial ECMs, Acta Biomater. 3 (5) (2007) 615–629.
[62] F. Grinnell, Fibroblast biology in three-dimensional collagen matrices, Trends Cell Biol. 13 (5) (2003) 264–269.
[63] K. Pogoda, P.A. Janmey, Glial tissue mechanics and mechanosensing by glial cells, Front. Cell. Neurosci. 12 (2018) 25.
[64] E. Moeendarbary, et al., The soft mechanical signature of glial scars in the central nervous system, Nat. Commun. 8 (2017) 14787.
[65] A. Buxboim, I.L. Ivanovska, D.E. Discher, Matrix elasticity, cytoskeletal forces and physics of the nucleus: how deeply do cells 'feel'outside and in?, J. Cell. Sci. 123 (3) (2010) 297–308.
[66] J. Swift, D.E. Discher, The nuclear lamina is mechano-responsive to ECM elasticity in mature tissue, J. Cell. Sci. 127 (14) (2014) 3005–3015.
[67] P.A. Janmey, et al., From tissue mechanics to transcription factors, Differentiation 86 (3) (2013) 112–120.
[68] J. Irianto, et al., Nuclear lamins in cancer, Cell. Mol. Bioeng. 9 (2) (2016) 258–267.
[69] X. Cao, et al., A chemomechanical model of matrix and nuclear rigidity regulation of focal adhesion size, Biophys. J. 109 (9) (2015) 1807–1817.
[70] B. Cheng, et al., Cellular mechanosensing of the biophysical microenvironment: A review of mathematical models of biophysical regulation of cell responses, Phys. Life Rev. (2017) S1571064517300878.
[71] G. Cao, J. Sui, S. Sun, Evaluating the nucleus effect on the dynamic indentation behavior of cells, Biomech. Model. Mechanobiol. 12 (1) (2013) 55–66.
[72] S. Joe, et al., Nuclear lamin-a scales with tissue stiffness and enhances matrix-directed differentiation, Science 341 (6149) (2013) 975.
[73] J.P. Marquez, G.M. Genin, Whole cell mechanics of contractile fibroblasts: relations between effective cellular and extracellular matrix moduli, Philos. Trans. 368 (1912) (2010) 635.